Title

Design and Structural Characterization of Potent and Selective Inhibitors of Phosphatidylinositol 4 Kinase IIIβ

Journal

Journal of Medicinal Chemistry, 59(5)

ISSN

0022-2623

Authors

Rutaganira, Florentine U
Fowler, Melissa L
McPhail, Jacob A
et al.

Publication Date

2016-03-10

DOI

10.1021/acs.jmedchem.5b01311

Peer reviewed

HHS Public Access

Author manuscript

J Med Chem. Author manuscript; available in PMC 2017 February 02.

Published in final edited form as:

J Med Chem. 2016 March 10; 59(5): 1830–1839. doi:10.1021/acs.jmedchem.5b01311.

Design and structural characterization of potent and selective inhibitors of phosphatidylinositol 4 kinase IIIβ

Florentine U. Rutaganira[1,a], **Melissa L. Fowler**[2,a], **Jacob A. McPhail**[2], **Michael A. Gelman**[3,%], **Khanh Nguyen**[3], **Anming Xiong**[3], **Gillian L. Dornan**[2], **Brandon Tavshanjian**[1], **Jeffrey S. Glenn**[3,4], **Kevan M. Shokat**[1,*], and **John E. Burke**[2,*]

[1]Howard Hughes Medical Institute and Department of Cellular and Molecular Pharmacology, University of California, San Francisco (UCSF), San Francisco, CA 94143, USA

[2]Department of Biochemistry and Microbiology, University of Victoria, Victoria BC, V8W 2Y2, Canada

[3]Departments of Medicine and Microbiology & Immunology, Stanford University, Palo Alto, CA 94305, USA

[4]Veterans Administration Medical Center, Palo Alto, CA, 94304

Abstract

Type III Phosphatidylinositol 4-kinase (PI4KIIIβ) is an essential enzyme in mediating membrane trafficking, and is implicated in a variety of pathogenic processes. It is a key host factor mediating replication of RNA viruses. The design of potent and specific inhibitors of this enzyme will be essential to define its cellular roles, and may lead to novel anti-viral therapeutics. We previously reported the PI4K inhibitor PIK93, and this compound has defined key functions of PI4KIIIβ. However, this compound showed high cross reactivity with class I and III PI3Ks. Using structure-based drug design we have designed novel potent and selective (>1000 fold over class I and class III PI3Ks) PI4KIIIβ inhibitors. These compounds showed anti-viral activity against Hepatitis C Virus. The co-crystal structure of PI4KIIIβ bound to one of the most potent compounds reveals the molecular basis of specificity. This work will be vital in the design of novel PI4KIIIβ inhibitors, which may play significant roles as anti-viral therapeutics.

Graphical Abstract

Corresponding Authors: Burke, John E. (jeburke@uvic.ca, 1-250-721-8732) and Shokat, Kevan M. (Kevan.Shokat@ucsf.edu, 1-415-514-0472).

[%]*Present/Current Author Addresses*: Department of Medicine, Veterans Administration Medical Center, Bronx, NY 10468

[a]These authors contributed equally.

ANCILLARY INFORRMATION

Supporting Information.

Supporting information including compound characterization, and two supplemental figures are found in the supplemental information, and this material is available free of charge via the *Internet at* http://pubs.acs.org.

PDB ID Codes: The structure factors and pdb coordinates have been deposited at the protein databank (PDB) with the coordinates 5EUQ.

Author Contributions

The manuscript was written through contributions of all authors. All authors have given approval to the final version of the manuscript.

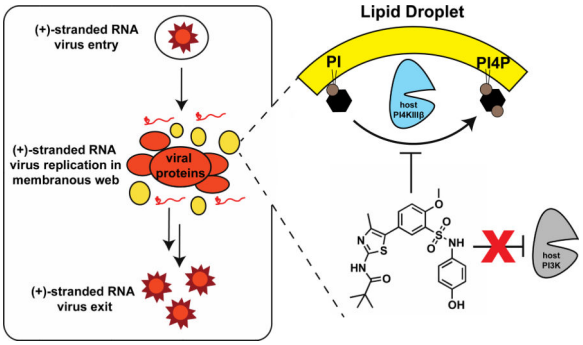

Introduction

Lipid phosphoinositides are essential regulators of myriad cellular processes, including signaling, membrane trafficking, and cytokinesis[1]. Phosphoinositides are generated through the phosphorylation of the inositol ring of phosphatidylinositol. Phosphatidylinositol can be phosphorylated and dephosphorylated by a diverse set of enzymes, and this results in a total of seven different mono and poly phosphorylated phosphoinositides. The lipid species phosphatidylinositol 4-phosphate (PI4P) is generated by the action of phosphatidylinositol 4 kinases (PI4Ks). PI4P is the main biosynthetic route for the multiply phosphorylated signaling lipids phosphatidylinositol 4,5-bisphosphate (PIP_2), and phosphatidylinositol 3,4,5-trisphosphate (PIP_3)[2]. In mammals there are four different PI4K enzymes, two type II enzymes (PI4KIIα and PI4KIIβ) and two type III enzymes (PI4KIIIα and PI4KIIIβ). PI4KIIIβ is a peripheral membrane protein that is primarily localized at the Golgi and the Trans Golgi Network (TGN). This enzyme plays key roles in mediating lipid transport[3], cytokinesis[4], maintaining lysosomal identity[5], and in tandem with Rab GTPases plays key roles in regulating membrane trafficking[6]. Interest in the development of potent small molecules of PI4KIIIβ has been driven recently by the discovery of the key role of this enzyme in both mediating viral replication[7], as well as in mediating *Plasmodium* development[8].

PI4KIIIβ is critical for mediating viral replication of a number of RNA viruses through the generation of PI4P enriched viral replication platforms. These membranous webs enriched in PI4P play essential roles in spatially concentrating viral replication proteins, and are key in intracellular viral replication. This process is essential for many human pathogenic viruses including Poliovirus, coxsackieviruses, Enterovirus 71, rhinovirus, and Aichi virus[7,9–13]. There is also evidence that PI4KIIIβ together with PI4KIIIα play a key role in mediating viral replication of Hepatitis C virus[13].

Small molecule inhibitors of PI4KIIIβ are potent anti-viral agents[7,14,15]. We previously reported the potent PI4KIIIβ inhibitor PIK93 (compound **1**)[16], and this compound has been used extensively to decipher the cellular roles of PI4KIIIβ[3,17], and its role in mediating viral replication of pathogenic RNA viruses[7,10–13]. Compound **1** potently inhibits PI4KIIIβ; however, it shows cross reactivity towards a number of other lipid kinases. Compound **1** has very similar IC50 values for PI4KIIIβ, class III PI3 kinase (vps34), and class IB PI3Kγ (Fig

1A). We have previously crystallized **1** in complex with PI4KIIIβ[18], vps34[19], and with PI3Kγ[16] (Fig. 1B–E).

Development of PI4KIIIβ as an effective drug target for anti-viral therapeutics requires the generation of highly potent and specific inhibitors. We report the development of a set of derivatives from compound **1**, and these represent some of the most potent PI4KIIIβ inhibitors reported to date. The selectivity profile of these compounds has been determined against vps34, PI3Kδ and PI3Kγ, with the most selective compounds being >1000 fold selective over the related PI3K family of lipid kinases. We have successfully determined the structure of PI4KIIIβ bound to one of the most potent and selective compounds, and this structure reveals the molecular basis for the increased selectivity and potency of these compounds.

Results

Design of optimized PI4KIIIβ inhibitors

Compound **1** is highly selective for PI4KIIIβ over PI4KIIIα, however, it is similarly potent for a number of phosphoinositide 3-kinases (PI3Ks), specifically the class I isoforms PI3Kγ (also referred to as p110γ) and PI3Kδ (also referred to as p110δ), as well as the class III PI3K vps34 (Fig. 1A). The structures of **1** bound to vps34[19], PI3Kγ[16], and PI4KIIIβ[18] revealed that within the binding pocket there were significant opportunities to modify **1** to increase both potency and selectivity for PI4KIIIβ.

From examining the structures of **1** bound to each enzyme, there were three regions of the molecule that were focused on to optimize both potency and selectivity of novel PI4KIIIβ inhibitors. These consisted of modifying the substituent on the central phenyl ring (colored green, Fig. 1A), the substituent off the sulfonamide (colored blue, Fig. 1A), and the acetamide moiety (colored red, Fig. 1 A). The chloro substituent on the central phenyl ring of **1** fits into a pocket partially composed of the activation loop of both PI3Ks and PI4KIIIβ (Fig. 1C). The conformation of the activation loop of PI3Kγ when bound to compound **1** is positioned closer to this substituent than in either vps34 or PI4KIIIβ. This suggested that modifying this group to a larger substituent might increase selectivity over class I PI3Ks. Changing this group to a bromo substituent (compound **2**) caused a slight increase in potency for PI4KIIIβ, PI3Kδ and vps34, and a slight decrease in potency for PI3Kγ. Modifying this group to a methoxy substituent (compound **3**) caused both an increase in potency for PI4KIIIβ and a large increase in specificity over PI3Kγ, PI3Kδ (>40 fold selective for both) and vps34 (Fig. 2A).

The structures of **1** bound to PI4KIIIβ, PI3Kγ, and vps34 also suggested that modification of the acetamide group derived from the central thiazole might lead to further gains in specificity. PI4KIIIβ has a much more open pocket around the acetamide group of **1** (Fig. 1C), compared to both PI3Kγ (Fig. 1D), and vps34 (Fig. 1E) which have a number of bulky hydrophobic residues. The methyl group of **1** was replaced with either a *t*-butyl group (compound **4**) or a cyclopentyl group (compound **5**). Both compounds showed similar or slightly better potency against PI4KIIIβ, however, both showed a very large increase in

selectivity over PI3Kγ (>600 fold for compound **4** and >90 fold for compound **5**), PI3Kδ, and vps34 (Fig. 2A).

Finally the ethanolamine attached to the sulfonamide in compound **1** was also derivatized. The ethanolamine was replaced with either a para-hydroxy phenol group (compound **6**) or a para-fluoro phenyl (compound **7**). The presence of the para-hydroxy phenol group caused a large increase in potency for all lipid kinases tested, with minimal differences in both potency and specificity for the para-fluoro phenyl substituent (Fig. 2A).

Combining this set of information we generated three compound **1** derivatives (compounds **8**+**9**+**10**) that contained derivations at multiple positions of **1**. All of these compounds contained a methoxy substituent off the central phenyl, with compound **9**+**10** containing a para-hydroxy phenol off the sulfonamide, and either a cylopentyl (compound **9**) or a *t*-butyl (compound **8**+**10**) group at the acetamide position off of the central thiazole. Both of the compounds containing the para hydroxyl phenol were extremely potent against PI4KIIIβ (IC50s of 7 nM and 3.6 nM for compound **9**+**10** respectively), and were >140 and >1000 fold selective over PI3Kγ, were >20 and >200 fold selective over PI3Kδ and showed no inhibition of vps34 at concentrations up to 20 μM (Fig. 2B). Compound **8** was not as potent (IC50 of 36 nM), but showed an excellent selectivity profile, with no inhibition of both PI3Kγ and vps34 (<20% at 50 μM), and very little inhibition of PI3Kδ (<50% inhibition at 50 μM). Compound **10** is the most potent PI4KIIIβ inhibitor currently reported; with very minor off-target inhibition of PI4KIIIβ related lipid kinases. Both compound **9**+**10** were further characterized against a panel of six additional lipid kinases (Fig. S1). Compound **9** showed weak inhibition of PI3KC2γ (IC50 ~1 μM), PI3Kα (~2 μM), and PI4KIIIα (~2.6 μM) and <50% inhibition at concentrations up to 20 μM for PI4K2α, PI4K2β, and PI3Kβ. Compound **10** showed weak inhibition of PI3KC2γ (IC50 ~1 μM), PI3Kα (~10 μM), and PI4KIIIα (~3 μM), and <20% inhibition at concentrations up to 20 μM for PI4K2α, PI4K2β, and PI3Kβ.

PI4KIIIβ has been shown to be a key host factor for the replication of the Hepatitis C virus[13,20]. To test the potency of the compound **1** derivative inhibitors as anti-virals we carried out viral replication assays using a luciferase reporter-linked infectious HCV clone. These results (Fig. 2, S2) generally show a trend of the most potent molecules being the most effective anti-virals, with increased specificity leading to decreased toxicity. One noticeable trend in the assay was that absence of the hydroxyl-phenyl group led to a large decrease in the anti-viral potency of the compounds. This may be due to differences in cell permeability caused by this group. The compounds with the best combination of anti-viral efficacy, and lowest toxicity were compounds **9** and **10** (Fig. S2).

Structural basis of specificity for PI4KIIIβ inhibitors

To determine the molecular basis for the potency and specificity of these novel PI4KIIIβ inhibitors we set out to crystallize them bound to PI4KIIIβ. We have previously crystallized a truncated construct of PI4KIIIβ in complex with compound **1** and the GTPase Rab11[18]. This structure revealed the molecular basis of its interaction with Rab11, as well as revealing the binding of compound **1** to PI4KIIIβ, however, this construct only crystallized in the

presence of compound **1**. To generate crystals of PI4KIIIβ bound to compound **9** we used a novel crystallization construct generated through the use of a hydrogen deuterium exchange mass spectrometry based approach[21]. This construct allowed us to generate crystals of PI4KIIIβ bound to GDP loaded Rab11 in the absence of inhibitors. These crystals were used to soak compound **9**, and allowed us to solve the co-crystal structure at 3.2 angstrom resolution. The binding mode of compound **9** was unambiguous (Fig. S3). The residues mediating contacts with compound **9** are shown in Fig. 3 A, with the shape of the inhibitor in the active site pocket shown in Fig. 3B.

Structure of PI4KIIIβ bound to compound 9

Compound **9** forms a crescent shape that conforms to the active site of PI4KIIIβ. This molecule makes extensive contacts with PI4KIIIβ (Fig 3A). There are two putative hydrogen bonds formed between the thiazole and the acetamide of compound **9** with both the amide and carbonyl group of V598. The sulfonamide group also forms a hydrogen bond with Lys549. All of these hydrogen bonds are similar to those reported in the structure of **1** bound to PI4KIIIβ[18]. Intriguingly the para-hydoxy group on the N-phenol sulfonamide also makes a putative hydrogen bond with the carbonyl of G660. The presence of this para hydroxyl group is important for potency, as molecules lacking this group are less potent against PI4KIIIβ (compound **6** versus compound **7**). The presence of this hydroxyl group also increases potency for both PI3Kγ and vps34 suggesting that this putative hydrogen bond is most likely conserved across all three enzymes.

The structure of compound **9** also reveals the molecular mechanism for how the acetamide and methoxy substituent mediate inhibitor selectivity over PI3Kγ and vps34. Aligning the structure of PI4KIIIβ bound to compound **9** with structures of compound **1** bound to PI3Kγ and vps34 (Figure 4A–C), reveals a number of steric clashes that explain the lack of potency of compound **9** against the PI3K family kinases. The acetamide group clashes with residues W812 and M953 in PI3Kγ, and residues Y746 and F673 in vps34. The methoxy group off the central phenyl group clashes with the aspartic acid from the DFG motif in the activation loop (D964 in PI3Kγ and D823 in vps34).

Discussion

Phosphatidylinositol 4 kinase IIIβ plays both key physiological and pathological roles, and the design of novel potent and selective inhibitors will be essential both in deciphering the cellular functions of this enzyme, as well as in the development of potential future therapeutic agents in diseases dependent on PI4KIIIβ activity. PI4KIIIβ mediates the replication of a variety of pathogenic RNA viruses, including members of both the *Picornaviridae* and *Flaviviridae* family of viruses[9]. These include viruses that pose significant threats to human health including SARS, MERS, Hepatitis C, and Polio. Along with this key role in mediating pathological conditions, PI4KIIIβ also plays key roles in a number of physiological roles including membrane trafficking[22], lipid transport[23], and cytokinesis[4] and the development of potent and selective molecules will be essential in deciphering the isoform specific functions of this enzyme.

Since PI4KIIIβ plays an essential role in mediating viral replication for a variety of pathogenic viruses, the development of PI4KIIIβ inhibitors has been an attractive target for pan anti-viral agents. A number of potent PI4KIIIβ inhibitors have recently been discovered[8,11,14,20,24–27], and experiments on a variety of RNA viruses show they are potent anti-viral agents. However, a complication of this work has been the toxic effects of some of these inhibitors on host function. There are conflicting results of the lethality of PI4KIIIβ inhibitors, with some showing lethality in mice[27], and others being well tolerated[14]. Deciphering if these effects are dependent on the inhibition of PI4KIIIβ, or through other off target effects requires the generation of novel more potent and specific PI4KIIIβ inhibitors. A specific goal for the development of antivirals is to avoid off target effects on both PI3Kγ and PI3Kδ as both of these enzymes play key roles in the immune system[28].

Here we describe a set of new compound **1** derivative inhibitors that are some of the most potent and specific PI4KIIIβ inhibitors as yet reported. Through a detailed structure based drug design approach we have designed derivatives that increased potency against PI4KIIIβ >5 fold while increasing selectivity >1000 fold to the related lipid kinases PI3Kγ and vps34. The most potent of these molecules (compound **10**) was screened over a panel of nine related lipid kinases and was >200 fold selective for PI4KIIIβ across all enzymes tested. Two of the most potent and selective molecules (compound **9**+**10**) were also the most effective antiviral compounds in a cellular model of Hepatitis C virus replication, with the best balance of antiviral potency and low cellular toxicity.

The structure of one of the most potent molecules bound to PI4KIIIβ was determined, and reveals the molecular basis for specificity of the derivative molecules. The pocket that accommodates the acetamide group of the inhibitors was found to be the most important region in mediating inhibitor selectivity, and the differences in the pocket accommodating this group in PI4KIIIβ compared to PI3Kγ and vps34 explains this observation. The acetamide group mediating specificity of PI4KIIIβ inhibitors strongly correlates with previous studies on compounds very similar to compound **1**. Addition of a bulky substituent in a similar position to the acetamide group in compound **1** had a limited role in potency, but greatly enhanced specificity[26,29]. Structural and computational models of a different class of inhibitors bound to PI4KIIIβ suggested an important role of the pocket located near this region in mediating both potency and selectivity[24]. The structural details of this compound bound in the active site pocket will provide a future framework for the modification of these compounds to modify the inhibitors in a way that will enhance their pharmacokinetic properties, but not lead to any decreases in their potency and specificity.

Experimental section

Protein Expression

Truncated human PI4KIIIβ (121–784 Δ249–287Δ408–507 S294A) (plasmid JM7) and full-length human Rab11a(Q70L) (plasmid pJB88) were expressed in BL21 C41 (DE3) cells. For Rab11a(Q70L) expression, cultures were grown to an OD_{600} of 0.7 and induced with 0.5 mM IPTG for 3.5 hours at 37 °C. For truncated PI4KIIIβ expression, cultures were induced overnight at 16 °C with 0.1 mM IPTG at an OD_{600} of 0.6. Cells were harvested by

centrifugation, washed with cold phosphate-buffered saline (PBS), frozen in liquid nitrogen, and pellets were stored at −80 °C.

Protein Purification

PI4KIIIβ (truncation) Purification—Cells were resuspended in 20 mM Tris-HCl pH 8.0, 100 mM NaCl, 10 mM imidazole, 5% (v/v) glycerol, 2 mM β-mercaptoethanol, and a 1:1666 dilution of a protease inhibitor cocktail (Milipore Protease Inhibitor Cocktail Set III, Animal-Free), and were sonicated on ice for 5 min with cycles consisting of 10 sec on, 10 sec off. Triton X-100 was then added to a final concentration of 0.2%, and the lysate was centrifuged for 45 min at 20,000 × g. The supernatant was then filtered through a 0.45 μm filter (Celltreat Scientific Products) and was loaded onto a 5 mL HisTrap FF column (GE Healthcare) equilibrated in buffer A (20 mM Tris-HCl pH 8.0, 100 mM NaCl, 10 mM imidazole, 5% (v/v) glycerol, 2 mM β-mercaptoethanol). The column was washed with 20 mL of buffer A, followed by 20 mL of 6% buffer B (20 mM Tris-HCl pH 8.0, 100 mM NaCl, 200 mM imidazole, 5% (v/v) glycerol, 2 mM β-mercaptoethanol), and was eluted with 100% buffer B. The His affinity tag protein was cleaved overnight at 4 °C with TEV protease. The cleaved protein was then diluted to 50 mM NaCl (using 20 mM Tris-HCl pH 8.0, 10 mM imidazole, 5% (v/v) glycerol, 2 mM β-mercaptoethanol) and was loaded onto a 5 mL HiTrap Q HP column (GE Healthcare) equilibrated in buffer C (20 mM Tris-HCl pH 8.0, 50 mM NaCl, 5% (v/v) glycerol, 2 mM β-mercaptoethanol). Protein was eluted with a gradient elution using buffer D (20 mM Tris-HCl pH 8.0, 1.0 M NaCl, 5% (v/v) glycerol, 2 mM β-mercaptoethanol). Fractions containing the cleaved PI4KIIIβ were pooled and concentrated to 700 μL in an Amicon 50K centrifugal filter (Millipore). The protein was then loaded onto a HiPrep 16/60 Sephacryl S200 column equilibrated in buffer E (20 mM HEPES pH 7.2, 150 mM NaCl, 1 mM TCEP). The cleaved PI4KIIIβ was then concentrated to approximately 15 mg/mL in an Amicon 50K centrifugal filter (Millipore), and aliquots were frozen in liquid nitrogen and stored at −80 °C.

Rab11a(Q70L) Purification—Cells were resuspended in 20 mM Tris-HCl pH 8.0, 100 mM NaCl, 5% (v/v) glycerol, 2 mM β-mercaptoethanol, and a 1:1666 dilution of a protease inhibitor cocktail (Milipore Protease Inhibitor Cocktail Set III, Animal-Free). Cells were sonicated and centrifuged as described for the truncated PI4KIIIβ. The supernatant was filtered through a 0.45 μm filter (Celltreat Scientific Products) and incubated for 1 hour with 4 mL of Glutathione Sepharose 4B beads (GE Healthcare) equilibrated in buffer F (20 mM Tris-HCl pH 8.0, 100 mM NaCl, 5% (v/v) glycerol, 2 mM β-mercaptoethanol) followed by a 3 × 15 mL wash in buffer F. The GST tag was cleaved overnight on the beads with TEV protease. Anion-exchange chromatography was performed as outlined above for the truncated PI4KIIIβ. Cleaved Rab11a(Q70L) were then concentrated to between 5–15 mg/mL and nucleotide loaded by adding EDTA to 10 mM followed by 1 U of phosphatase (Phosphatase, Alkaline-Agarose from calf intestine, Sigma P0762-100UN) per mg of protein. Proteins were then incubated for 1.5 hours. The phosphatase was removed using a 0.2 μm spin filter (Millipore); the flow-through was collected, and a 10-fold molar excess of GDP was added followed by $MgCl_2$ to a final concentration of 20 mM. Proteins were incubated for 30 min. Gel filtration was performed with cleaved GDP-loaded Rab11a(Q70L) as described above for the truncated PI4KIIIβ.

Crystallography

Crystals of PI4KIIIβ (final concentration 7.4 mg/mL) with Rab11a–GDP (final concentration 4.5 mg/mL) were obtained in 15% (w/v) PEG-4000, 100 mM sodium citrate pH 5.6, 200 mM ammonium sulfate (protein:precipitant ratio of 3:1). Refinement plates were set by gridding PEG-4000, ammonium sulfate, and glycerol. Optimized crystals were obtained by seeding using the Hampton Research Seed Bead Kit according to the manufacturer's instructions using a reservoir solution of 14.8% (w/v) PEG-4000, 100 mM sodium citrate pH 5.6, 250 mM ammonium sulfate. The best crystals were obtained in 13–15% (w/v) PEG-4000, 100 mM sodium citrate pH 5.6, 250 mM ammonium sulfate, 2% glycerol with a 1/1000 or 1/10,000 seed solution dilution, a Rab11a–GDP final concentration of 4.51 mg/mL and a PI4KIIIβ final concentration of 7.38 mg/mL. Crystals were frozen in liquid nitrogen using a 15% PEG-4000 (w/v), 100 mM sodium citrate pH 5.6, 250 mM ammonium sulfate, 25% (v/v) glycerol cryo solution.

Inhibitor soaks were performed by incubating crystals with 0.5 μL of 10 μM inhibitor stocks in cryo buffer (15% PEG-4000 (w/v), 250 mM ammonium sulfate, 100 mM sodium citrate pH 5.6, 25% glycerol (v/v)) for 30 min, followed by a 30 min incubation with 0.5 μL of 100 μM inhibitor stock in cryo buffer, and a final 30 min incubation in 1 mM inhibitor stock in cryo buffer. Before the final addition, 1 μL was removed from the crystal drop and 1 μL of the 1 mM inhibitor in cryo buffer was added.

Diffraction data were collected at 100 K at the Canadian Macromolecular Crystallography Facility (Canadian Light Source, CLS) beamline 08ID-1. Data were integrated using iMosflm 7.1.1[30] and scaled with AIMLESS[31]. Phases were initially obtained by molecular replacement (MR) using Phaser[32], with the structure of PI4KIIIβ bound to compound **1** and Rab11 (pdb code: 4D0L) used as the search model. The final model of PI4KIIIβ bound to compound **9** in complex with Rab11 was built using iterative model building in COOT[33] and refinement using Phenix[34,35] to R_{work}=23.87 and R_{free}=26.79. The binding mode of compound **9** was unambiguous, and ligand geometry was generated using the elbow subset of Phenix[36]. Full crystallographic statistics are shown in Table 1.

Biochemical Assays

Lipid kinase assays were preformed using recombinant enzyme, phosphoinositides purchased from Avanti Polar Lipids and γ^{32}P-ATP (Perkin Elmer Cat #BLU502A001MC) in a membrane capture assay described previously[37]. Each inhibitor was diluted into 10% DMSO and kinase assay buffer. Upon completion of the reaction, 4 μL was spotted onto 0.2μm nitrocellulose (Bio-Rad Catalog #162-0112). The membrane was dried for 5 minutes under a heat lamp followed by 1×30 second wash and 6×5 min washes in 1M NaCl / 1% Phosphoric Acid. The membrane was dried for 20 minutes under a heat lamp followed by overnight exposure to a phosphor screen and phosphorimaging followed on a Typhoon 9500. Intensities were quantified using SPOT[37]. Specifications for each enzyme follow.

PI4KIIIβ

Recombinant enzyme was purchased from Life Technologies (Cat # PV5277, Lot 943589E). L-α-Phosphatidylinositol (PI, Cat # 840024P) and DOPS:DOPC lipids (Cat # 790595P)

were sonicated in water to generate 1mg/mL PI:DOPS:DOPC. Reaction was set-up as follows 1) kinase assay buffer, PI:DOPS:DOPC, BSA and PI4KIIIβ, were combined in a total volume of 10 μL (2.5x solution); 2) 5 μL of inhibitor solution was added (5x solution) and incubated with enzyme mixture for 15 minutes; 3) 10 μL cold ATP and γ^{32}P-ATP were added (2.5x solution) to initiate the reaction which ran for 30 minutes. Final conditions were as follows: 20mM Bis-Tris Propane pH 7.5, 10mM $MgCl_2$, 0.075mM Triton X-100, 0.5mM EGTA, 1mM DTT, 100μM PI, 500ng/μL BSA, 2.5nM PI4KIIIβ, 2% DMSO, 10μM ATP and 1uCi γ^{32}P-ATP.

PI3Kγ

Recombinant enzyme was purchased from Life Technologies (Cat # PV4786, Lot # 1638926A). L-α-Phosphatidylinositol-4,5-bisphosphate (PIP_2, Cat # 840046P) and DOPS:DOPC lipids (Cat # 790595P) were sonicated in water to generate 1mg/mL PIP_2:DOPS:DOPC. Reaction was set-up as follows 1) kinase assay buffer, PIP_2:DOPS:DOPC, BSA and PI3Kγ, were combined in a total volume of 10 μL (2.5x solution); 2) 5 μL of inhibitor solution was added (5x solution) and incubated with enzyme mixture for 15 minutes; 3) 10 μL cold ATP and γ^{32}P-ATP were added (2.5x solution) to initiate the reaction which ran for 15 minutes. Final conditions were as follows: 50mM HEPES pH 7.5, 100mM NaCl, 0.03% CHAPS, 10mM $MgCl_2$, 1mM EGTA, 2mM DTT, 5nM PI3Kγ, 80μM PIP_2, 500ng/ μL BSA, 2% DMSO, 10μM ATP and 1uCi γ^{32}P-ATP.

PI3Kβ

Recombinant enzyme was purchased from Life Technologies (Cat # PV6451, Lot # 1763224). L-α-Phosphatidylinositol-4,5-bisphosphate (PIP_2, Cat # 840046P) and DOPS:DOPC lipids (Cat # 790595P) were sonicated in water to generate 1mg/mL PIP_2:DOPS:DOPC. Reaction was set-up as follows 1) kinase assay buffer, PIP_2:DOPS:DOPC, BSA and PI3Kδ, were combined in a total volume of 10 μL (2.5x solution); 2) 5 μL of inhibitor solution was added (5x solution) and incubated with enzyme mixture for 15 minutes; 3) 10 μL cold ATP and γ^{32}P-ATP were added (2.5x solution) to initiate the reaction which ran for 20 minutes. Final conditions were as follows: 50mM HEPES pH 7.5, 100mM NaCl, 0.03% CHAPS, 10mM $MgCl_2$, 1mM EGTA, 2mM DTT, 2.5nM PI3Kδ, 80μM PIP_2, 500ng/ μL BSA, 2% DMSO, 10μM ATP and 2.5uCi γ^{32}P-ATP.

vps34

Recombinant enzyme was purchased from Life Technologies (Cat # PV5126, Lot # 1555138A). L-α-Phosphatidylinositol (PI, Cat # 840024P) and DOPS:DOPC lipids (Cat # 790595P) were sonicated in water to generate 1mg/mL PI:DOPS:DOPC. Reaction was set-up as follows 1) kinase assay buffer, PI:DOPS:DOPC, BSA and vps34, were combined in a total volume of 10 μL (2.5x solution); 2) 5 μL of inhibitor solution was added (5x solution) and incubated with enzyme mixture for 15 minutes; 3) 10 μL cold ATP and γ^{32}P-ATP were added (2.5x solution) to initiate the reaction which ran for 1 hour. Final conditions were as follows: 50mM HEPES pH 7.5, 0.1% CHAPS, 2mM $MnCl_2$, 1mM EGTA, 2mM DTT, 10nM vps34, 100μM PI, 500ng/ μL BSA, 2% DMSO, 10μM ATP and 2.5uCi γ^{32}P-ATP.

PI4KIIIα

Recombinant enzyme was purchased from EMD Millipore (Cat # 14–908, Lot # D9KN031N–B). L-α-Phosphatidylinositol (PI, Cat # 840024P) and DOPS:DOPC lipids (Cat # 790595P) were sonicated in water to generate 1mg/mL PI:DOPS:DOPC. Reaction was set-up as follows 1) kinase assay buffer, PI:DOPS:DOPC, BSA and PI4KIIIα, were combined in a total volume of 10 μL (2.5x solution); 2) 5 μL of inhibitor solution was added (5x solution) and incubated with enzyme mixture for 15 minutes; 3) 10 μL cold ATP and γ^{32}P-ATP were added (2.5x solution) to initiate the reaction which ran for 25 minutes. Final conditions were as follows: 20mM Bis-Tris Propane pH 7.5, 10mM $MgCl_2$, 0.075mM Triton X-100, 0.5mM EGTA, 1mM DTT, 100μM PI, 500ng/μL BSA, 1.2nM PI4KIIIα, 2% DMSO, 10μM ATP and 2uCi γ^{32}P-ATP.

PI4KIIα

PI4KIIα was cloned from DNASU plasmid HsCD00003332[38,39]. Recombinant enzyme was obtained through FLAG immunoprecipitation of FLAG-PI4KIIα transfected into HEK293T cells (10ug of FLAG-PI4KIIα transfected with Life Technologies Lipofectamine and Plus Reagent to a 15cm dish of HEK293Ts and 75uL elution with FLAG peptide). L-α-Phosphatidylinositol (PI, Cat # 840024P) and DOPS:DOPC lipids (Cat # 790595P) were sonicated in water to generate 1mg/mL PI:DOPS:DOPC. Reaction was set-up as follows 1) kinase assay buffer, PI:DOPS:DOPC, BSA and PI4KIIα, were combined in a total volume of 10 μL (2.5x solution); 2) 5 μL of inhibitor solution was added (5x solution) and incubated with enzyme mixture for 15 minutes; 3) 10 μL cold ATP and γ^{32}P-ATP were added (2.5x solution) to initiate the reaction which ran for 25 minutes. Final conditions were as follows: 20mM Bis-Tris Propane pH 7.5, 10mM $MgCl_2$, 0.075mM Triton X-100, 0.5mM EGTA, 1mM DTT, 100μM PI, 500ng/μL BSA, 2.9uL PI4KIIα, 2% DMSO, 10μM ATP and 2uCi γ^{32}P-ATP.

PI4KIIβ

PI4KIIβ was cloned from DNASU plasmid HsCD00001592[38,39]. Recombinant enzyme was obtained through FLAG immunoprecipitation of FLAG-PI4KIIβ transfected into HEK293T cells (10ug of FLAG-PI4KIIβ transfected with Life Technologies Lipofectamine and Plus Reagent to a 15cm dish of HEK293Ts and 75uL elution with FLAG peptide). L-α-Phosphatidylinositol (PI, Cat # 840024P) and DOPS:DOPC lipids (Cat # 790595P) were sonicated in water to generate 1mg/mL PI:DOPS:DOPC. Reaction was set-up as follows 1) kinase assay buffer, PI:DOPS:DOPC, BSA and PI4KIIβ, were combined in a total volume of 10 μL (2.5x solution); 2) 5 μL of inhibitor solution was added (5x solution) and incubated with enzyme mixture for 15 minutes; 3) 10 μL cold ATP and γ^{32}P-ATP were added (2.5x solution) to initiate the reaction which ran for 25 minutes. Final conditions were as follows: 20mM Bis-Tris Propane pH 7.5, 10mM $MgCl_2$, 0.075mM Triton X-100, 0.5mM EGTA, 1mM DTT, 100μM PI, 500ng/μL BSA, 2uL PI4KIIβ, 2% DMSO, 10μM ATP and 2uCi γ^{32}P-ATP.

PI3Kα

Recombinant enzyme was purchased from EMD Millipore (Cat # 14–602, Lot # 2150294-A). L-α-Phosphatidylinositol-4,5-bisphosphate (PIP_2, Cat # 840046P) and DOPS:DOPC lipids (Cat # 790595P) were sonicated in water to generate 1mg/mL PIP_2:DOPS:DOPC. Reaction was set-up as follows 1) kinase assay buffer, PIP_2:DOPS:DOPC, BSA and PI3Kα, were combined in a total volume of 10 μL (2.5x solution); 2) 5 μL of inhibitor solution was added (5x solution) and incubated with enzyme mixture for 15 minutes; 3) 10 μL cold ATP and γ^{32}P-ATP were added (2.5x solution) to initiate the reaction which ran for 15 minutes. Final conditions were as follows: 50mM HEPES pH 7.5, 100mM NaCl, 0.03% CHAPS, 10mM $MgCl_2$, 1mM EGTA, 2mM DTT, 3.3nM PI3Kα, 80μM PIP_2, 500ng/ μL BSA, 2% DMSO, 10μM ATP and 2uCi γ^{32}P-ATP.

PI3Kβ

Recombinant enzyme was purchased from SignalChem (Cat # P28-10H-10, Lot # F-532-3). L-α-Phosphatidylinositol-4,5-bisphosphate (PIP_2, Cat # 840046P) and DOPS:DOPC lipids (Cat # 790595P) were sonicated in water to generate 1mg/mL PIP_2:DOPS:DOPC. Reaction was set-up as follows 1) kinase assay buffer, PIP_2:DOPS:DOPC, BSA and PI3Kβ, were combined in a total volume of 10 μL (2.5x solution); 2) 5 μL of inhibitor solution was added (5x solution) and incubated with enzyme mixture for 15 minutes; 3) 10 μL cold ATP and γ^{32}P-ATP were added (2.5x solution) to initiate the reaction which ran for 15 minutes. Final conditions were as follows: 50mM HEPES pH 7.5, 100mM NaCl, 0.03% CHAPS, 10mM $MgCl_2$, 1mM EGTA, 2mM DTT, 0.6nM PI3Kβ, 80μM PIP_2, 500ng/ μL BSA, 2% DMSO, 10μM ATP and 2uCi γ^{32}P-ATP.

PI3KC2γ

Recombinant enzyme was purchased from EMD Millipore (Cat # 14–910, Lot # 2023057-A). L-α-Phosphatidylinositol (PI, Cat # 840024P) and DOPS:DOPC lipids (Cat # 790595P) were sonicated in water to generate 1mg/mL PI:DOPS:DOPC. Reaction was set-up as follows 1) kinase assay buffer, PI:DOPS:DOPC, BSA and PI3KC2γ, were combined in a total volume of 10 μL (2.5x solution); 2) 5 μL of inhibitor solution was added (5x solution) and incubated with enzyme mixture for 15 minutes; 3) 10 μL cold ATP and γ^{32}P-ATP were added (2.5x solution) to initiate the reaction which ran for 15 minutes. Final conditions were as follows: 50mM HEPES pH 7.5, 100mM NaCl, 0.03% CHAPS, 10mM $MgCl_2$, 1mM EGTA, 2mM DTT, 1nM PI3KC2γ, 100μM PI, 500ng/ μL BSA, 2% DMSO, 10μM ATP and 2uCi γ^{32}P-ATP.

Organic Synthesis

Materials obtained commercially were reagent grade and were used without further purification. ^{1}H NMR spectra were recorded on a Varian 400 spectrometer at 400 MHz . High-resolution electron impact mass spectra were recorded on a Thermo Fisher Exactive EMR and Thermo Fisher LTQ Orbitrap Velos at the University of California-San Francisco center for Mass Spectrometry. Reactions were monitored by thin layer chromatography (TLC), using Merck silica gel 60 F254 glass plates (0.25 mm thick). Flash chromatography was conducted with Grace Reveleris flash cartridges with 40μm silica on an Agilent 971-FP.

All RP-HPLC were performed with a Waters 2545 binary gradient module equipped with an XBridge prep C18 column using H2O + 0.1% formic acid and CH3CN + 0.1% formic acid (5–95% gradient) while monitoring at 254 nm. All final compounds were >95% pure as measured by Liquid Chromatography Mass Spectrometry (LCMS). Full compound characterization details are presented in the supporting information.

Synthesis of compound **1** and derivatives was conducted similarly to methods described previously[16], and is shown in scheme 1. To commercially available acetaphenone chlorosulfuric acid (11eq) was added dropwise in an ice bath and the reaction was heated to 40°C for 2 hours. The reaction was stopped by dropwise transfer to ice-water. The aqueous phase was extracted 3x with ethyl acetate and the combined organic is dried with sodium sulfate, filtered and concentrated *in vacuo* to give a brown oil, the crude corresponding to sulfonyl chloride, **A**. The sulfonyl chloride was dissolved in THF (1.5M), the appropriate amino alcohol (4.5eq) was added and the reaction was allowed to stir overnight at room temperature. The reaction was concentrated *in vacuo*, water is added and the aqueous phase was extracted 3x with ethyl acetate. The combined organic phase was concentrated and intermediate **B** was purified using silica gel flash chromatography (2% - 10% methanol in dichloromethane). If pure intermediate was not obtained, the intermediate was subjected to a second purification by reverse phase HPLC using acetonitrile/water/0.1% formic acid as a solvent system.

Intermediate **B** was dissolved in THF (1.5M). (2-carboxyethyl) triphenylphosphonium bromide was dissolved in THF (1M) and intermediate **B** was added to the bromide solution dropwise at room temperature. The reaction was allowed to proceed 1 hour at room temperature and the solvent is removed *in vacuo* and the product was purified by silica gel flash chromatography (0% - 10% methanol in dichloromethane) to yield intermediate **C**.

To ethanol-recrystallized thiourea in dry toluene (0.5M) was added appropriate acyl chloride and the reaction was heated to reflux for 18 hours. Toluene was removed *in vacuo* and the reaction was diluted in ethyl acetate and filtered. The organic layer was washed 2x with water and dried with brine and sodium sulfate and reduced *in vacuo*. The resulting acetylthiourea **D** was purified by silica gel flash chromatography (25% - 100% ethyl acetate in hexanes).

Intermediate **C** was dissolved in ethanol (0.17M) and appropriate acetylthiourea **D** was added at room temperature. The reaction was heated to reflux for 30 minutes and then cooled to room temperature and compound **1** or compound **1** derivative was purified by silica gel chromatography (0% - 10% methanol in dichloromethane) and if necessary, followed by reverse phase HPLC using acetonitrile/water/0.1% formic acid as a solvent system.

Gaussia luciferase-based HCV reporter virus and stable cell line of Huh7.5 containing infectious HCV reporter virus

A fully-infectious HCVcc genotype 2a reporter virus encoding *Gaussia* luciferase between p7 and NS2 similar to Maurkian et al. [40] was generated to monitor HCV replication quantitatively. Briefly, *Gaussia* luciferase gene with an in frame foot and mouth disease virus

autoproteolytic 2A peptide sequence was inserted between HCV p7 and NS2 of a J6/JFH1 infectious HCV clone [41], resulting in the fully-infectious HCVcc reporter virus J6/JFH1-GLuc (p7-NS2-GLucFM2A). After Huh7.5 cells were infected with the Gaussia luciferase-based HCV reporter virus, the cells were maintained for three days and then passed every four days for twenty passages. A stable cell line with consistent Gaussia luciferase secretion was established.

HCV2a antiviral assay

Huh 7.5 cells stably infected with J6/JFH1-GLuc were maintained and passaged in DMEM (Mediatech, Manassas, VA) supplemented with 10% FBS (Omega Scientific, Tarzana, CA), 2 mM glutamine (Mediatech, Manassas, VA), non-essential amino acids (Mediatech, Manassas, VA), 100 IU/mL penicillin (Mediatech, Manassas, VA), and 100 g/mL streptomycin (Mediatech, Manassas, VA) in 37°C incubator with 5% CO2 and 95% relative humidity.

Ten thousand cells were plated in 96 well plates (E&K Scientific Products, Santa Clara, CA) and supplemented with serially diluted compounds one hour after plating. After three days incubation, viability was tested using the Presto Blue cell viability reagent (Life Technologies Corporation, Grand Island, NY) per the manufacturer's protocol and replication was measured by determining the Gaussia luciferase activity in the supernatant using the luciferase reagent (Promega Corporation, Madison, WI) according to the manufacturer's protocol.

Viability and luminescence were read using a plate reader (Infinite 1000, Tecan Systems, San Jose, CA). Values were imported into Prism (GraphPad Software, La Jolla, CA) for graphing and calculations of EC50 and CC50 values.

Supplementary Material

Refer to Web version on PubMed Central for supplementary material.

Acknowledgments

J.E.B. wishes to thank CIHR support (CIHR new investigator grant and CIHR open operating grant FRN 142393). K.M.S. and J.S.G. wish to thank NIH support (R01 AI099245 and U19 AI109622). M.A.G. wishes to thank NIH support (K08 AI097322).

We thank the staff at the Canadian Light Source (CLS) CMCF-ID beam line where diffraction data were collected. The CLS is supported by the Natural Sciences and Engineering Research Council of Canada, the National Research Council Canada, the Canadian Institutes of Health Research, the Province of Saskatchewan, Western Economic Diversification Canada, and the University of Saskatchewan. High Resolution Mass Spectrometry was provided by the Bio-Organic Biomedical Mass Spectrometry Resource at UCSF (A.L. Burlingame, Director) supported by the Biomedical Technology Research Centers program of the NIH National Institute of General Medical Sciences, NIH NIGMS 8P41GM103481 and NIH 1S10OD016229 and the Howard Hughes Medical Institute.

Abbreviations

PI4K	Phosphatidylinositol 4 kinase
PI3K	phosphoinositide 3 kinase

PI4P	phosphatidylinositol 4-phosphate
PIP_2	phosphatidylinositol 4,5-bisphosphate
PIP_3	phosphatidylinositol 3,4,5-trisphosphate

REFERENCES

1. Balla T. Phosphoinositides: Tiny Lipids with Giant Impact on Cell Regulation. Physiol. Rev. 2013; 93:1019–1137. [PubMed: 23899561]
2. Tan J, Brill JA. Cinderella Story: PI4P Goes From Precursor to Key Signaling Molecule. Crit. Rev. Biochem. Mol. Biol. 2014; 49:33–58. [PubMed: 24219382]
3. Tóth B, Balla A, Ma H, Knight ZA, Shokat KM, Balla T. Phosphatidylinositol 4-Kinase IIIbeta Regulates the Transport of Ceramide Between the Endoplasmic Reticulum and Golgi. J. Biol. Chem. 2006; 281:36369–36377. [PubMed: 17003043]
4. Polevoy G, Wei H-C, Wong R, Szentpetery Z, Kim YJ, Goldbach P, Steinbach SK, Balla T, Brill JA. Dual Roles for the Drosophila PI 4-Kinase Four Wheel Drive in Localizing Rab11 During Cytokinesis. J. Cell Biol. 2009; 187:847–858. [PubMed: 19995935]
5. Sridhar S, Patel B, Aphkhazava D, Macian F, Santambrogio L, Shields D, Cuervo AM. The Lipid Kinase PI4KIIIβ Preserves Lysosomal Identity. EMBO J. 2013; 32:324–339. [PubMed: 23258225]
6. Jean S, Kiger AA. Coordination Between RAB GTPase and Phosphoinositide Regulation and Functions. Nat. Rev. Mol. Cell Biol. 2012; 13:463–470. [PubMed: 22722608]
7. Hsu N-Y, Ilnytska O, Belov G, Santiana M, Chen Y-H, Takvorian PM, Pau C, van der Schaar H, Kaushik-Basu N, Balla T, Cameron CE, Ehrenfeld E, van Kuppeveld FJM, Altan-Bonnet N. Viral Reorganization of the Secretory Pathway Generates Distinct Organelles for RNA Replication. Cell. 2010; 141:799–811. [PubMed: 20510927]
8. McNamara CW, Lee MCS, Lim CS, Lim SH, Roland J, Nagle A, Simon O, Yeung BKS, Chatterjee AK, McCormack SL, Manary MJ, Zeeman AM, Dechering KJ, Kumar TRS, Henrich PP, Gagaring K, Ibanez M, Kato N, Kuhen KL, Fischli C, Rottmann M, Plouffe DM, Bursulaya B, Meister S, Rameh L, Trappe J, Haasen D, Timmerman M, Sauerwein RW, Suwanarusk R, Russell B, Renia L, Nosten F, Tully DC, Kocken CHM, Glynne RJ, Bodenreider C, Fidock DA, Diagana TT, Winzeler EA. Targeting Plasmodium PI(4)K to Eliminate Malaria. Nature. 2013; 504:248–253. [PubMed: 24284631]
9. Altan-Bonnet N, Balla T. Phosphatidylinositol 4-Kinases: Hostages Harnessed to Build Panviral Replication Platforms. Trends in Biochemical Sciences. 2012; 37:293–302. [PubMed: 22633842]
10. Mello C, Aguayo E, Rodriguez M, Lee G, Jordan R, Cihlar T, Birkus G. Multiple Classes of Antiviral Agents Exhibit in Vitro Activity Against Human Rhinovirus Type C. Antimicrob. Agents Chemother. 2014; 58:1546–1555. [PubMed: 24366736]
11. van der Schaar HM, van der Linden L, Lanke KHW, Strating JRPM, Pürstinger G, de Vries E, de Haan CAM, Neyts J, van Kuppeveld FJM. Coxsackievirus Mutants That Can Bypass Host Factor PI4KIIIβ and the Need for High Levels of PI4P Lipids for Replication. Cell Res. 2012; 22:1576–1592. [PubMed: 22945356]
12. Greninger AL, Knudsen GM, Betegon M, Burlingame AL, DeRisi JL. The 3A Protein From Multiple Picornaviruses Utilizes the Golgi Adaptor Protein ACBD3 to Recruit PI4KIIIβ. J. Virol. 2012; 86:3605–3616. [PubMed: 22258260]
13. Borawski J, Troke P, Puyang X, Gibaja V, Zhao S, Mickanin C, Leighton-Davies J, Wilson CJ, Myer V, Cornellataracido I, Baryza J, Tallarico J, Joberty G, Bantscheff M, Schirle M, Bouwmeester T, Mathy JE, Lin K, Compton T, Labow M, Wiedmann B, Gaither LA. Class III Phosphatidylinositol 4-Kinase Alpha and Beta Are Novel Host Factor Regulators of Hepatitis C Virus Replication. J. Virol. 2009; 83:10058–10074. [PubMed: 19605471]
14. van der Schaar HM, Leyssen P, Thibaut HJ, de Palma A, van der Linden L, Lanke KHW, Lacroix C, Verbeken E, Conrath K, Macleod AM, Mitchell DR, Palmer NJ, van de Poël H, Andrews M, Neyts J, van Kuppeveld FJM. A Novel, Broad-Spectrum Inhibitor of Enterovirus Replication That

Targets Host Cell Factor Phosphatidylinositol 4-Kinase IIIβ. Antimicrob. Agents Chemother. 2013; 57:4971–4981. [PubMed: 23896472]

15. Arita M, Kojima H, Nagano T, Okabe T, Wakita T, Shimizu H. Phosphatidylinositol 4-Kinase III Beta Is a Target of Enviroxime-Like Compounds for Antipoliovirus Activity. J. Virol. 2011; 85:2364–2372. [PubMed: 21177810]
16. Knight Z, Gonzalez B, Feldman M, Zunder E, Goldenberg D, Williams O, Loewith R, Stokoe D, Balla A, Toth B, Balla T, Weiss W, Williams R, Shokat K. A Pharmacological Map of the PI3-K Family Defines a Role for P110alpha in Insulin Signaling. Cell. 2006; 125:733–747. [PubMed: 16647110]
17. Balla A, Kim YJ, Várnai P, Szentpetery Z, Knight Z, Shokat KM, Balla T. Maintenance of Hormone-Sensitive Phosphoinositide Pools in the Plasma Membrane Requires Phosphatidylinositol 4-Kinase IIIalpha. Mol. Biol. Cell. 2008; 19:711–721. [PubMed: 18077555]
18. Burke JE, Inglis AJ, Perisic O, Masson GR, McLaughlin SH, Rutaganira F, Shokat KM, Williams RL. Structures of PI4KIIIβ Complexes Show Simultaneous Recruitment of Rab11 and Its Effectors. Science. 2014; 344:1035–1038. [PubMed: 24876499]
19. Miller S, Tavshanjian B, Oleksy A, Perisic O, Houseman B, Shokat K, Williams R. Shaping Development of Autophagy Inhibitors with the Structure of the Lipid Kinase Vps34. Science. 2010; 327:1638–1642. [PubMed: 20339072]
20. Lamarche MJ, Borawski J, Bose A, Capacci-Daniel C, Colvin R, Dennehy M, Ding J, Dobler M, Drumm J, Gaither LA, Gao J, Jiang X, Lin K, McKeever U, Puyang X, Raman P, Thohan S, Tommasi R, Wagner K, Xiong X, Zabawa T, Zhu S, Wiedmann B. Anti-Hepatitis C Virus Activity and Toxicity of Type III Phosphatidylinositol-4-Kinase Beta Inhibitors. Antimicrob. Agents Chemother. 2012; 56:5149–5156. [PubMed: 22825118]
21. Fowler ML, McPhail JA, Jenkins ML, Masson GR, Rutaganira FU, Shokat KM, Williams RL, Burke JE. Using Hydrogen Deuterium Exchange Mass Spectrometry to Engineer Optimized Constructs for Crystallization of Protein Complexes: Case Study of PI4KIIIβ with Rab11. *Protein Sci*. Online early access. Published online: Jan 12, 2016.
22. Jovic M, Kean MJ, Szentpetery Z, Polevoy G, Gingras A-C, Brill JA, Balla T. Two Phosphatidylinositol 4-Kinases Control Lysosomal Delivery of the Gaucher Disease Enzyme, B-Glucocerebrosidase. Mol. Biol. Cell. 2012; 23:1533–1545. [PubMed: 22337770]
23. D'Angelo G, Vicinanza M, Wilson C, De Matteis MA. Phosphoinositides in Golgi Complex Function. Subcell. Biochem. 2012; 59:255–270. [PubMed: 22374093]
24. Mejdrová I, Chalupská D, Kögler M, Šála M, Plačková P, Baumlová A, Hřebabecký H, Procházková E, Dejmek M, Guillon R, Strunin D, Weber J, Lee G, Birkus G, Mertlíková-Kaiserová H, Boura E, Nencka R. Highly Selective Phosphatidylinositol 4-Kinase IIIβ Inhibitors and Structural Insight Into Their Mode of Action. J. Med. Chem. 2015; 58:3767–3793. [PubMed: 25897704]
25. Arita M, Philipov S, Galabov AS. Phosphatidylinositol 4-Kinase III Beta Is the Target of Oxoglaucine and Pachypodol (Ro 09-0179) for Their Anti-Poliovirus Activities, and Locates at Upstream of the Target Step of Brefeldin a. Microbiol. Immunol. 2015
26. Waring MJ, Andrews DM, Faulder PF, Flemington V, McKelvie JC, Maman S, Preston M, Raubo P, Robb GR, Roberts K, Rowlinson R, Smith JM, Swarbrick ME, Treinies I, Winter JJG, Wood RJ. Potent, Selective Small Molecule Inhibitors of Type III Phosphatidylinositol-4-Kinase A- but Not B-Inhibit the Phosphatidylinositol Signaling Cascade and Cancer Cell Proliferation. Chem. Commun. (Camb.). 2014; 50:5388–5390. [PubMed: 24366037]
27. Spickler C, Lippens J, Laberge M-K, Desmeules S, Bellavance É, Garneau M, Guo T, Hucke O, Leyssen P, Neyts J, Vaillancourt FH, Décor A, O'Meara J, Franti M, Gauthier A. Phosphatidylinositol 4-Kinase III Beta Is Essential for Replication of Human Rhinovirus and Its Inhibition Causes a Lethal Phenotype in Vivo. Antimicrob. Agents Chemother. 2013; 57:3358–3368. [PubMed: 23650168]
28. Okkenhaug K. Signaling by the Phosphoinositide 3-Kinase Family in Immune Cells. Annu. Rev. Immunol. 2013; 31:675–704. [PubMed: 23330955]
29. Keaney EP, Connolly M, Dobler M, Karki R, Honda A, Sokup S, Karur S, Britt S, Patnaik A, Raman P, Hamann LG, Wiedmann B, LaMarche MJ. 2-Alkyloxazoles as Potent and Selective

PI4KIIIβ Inhibitors Demonstrating Inhibition of HCV Replication. Bioorganic & Medicinal Chemistry Letters. 2014; 24:3714–3718. [PubMed: 25065492]

30. Battye TGG, Kontogiannis L, Johnson O, Powell HR, Leslie AGW. iMOSFLM: a New Graphical Interface for Diffraction-Image Processing with MOSFLM. Acta Crystallogr. D Biol. Crystallogr. 2011; 67:271–281. [PubMed: 21460445]
31. Evans PR, Murshudov GN. How Good Are My Data and What Is the Resolution? Acta Crystallogr. D Biol. Crystallogr. 2013; 69:1204–1214. [PubMed: 23793146]
32. McCoy AJ, Grosse-Kunstleve RW, Adams PD, Winn MD, Storoni LC, Read RJ. Phaser Crystallographic Software. J. Appl. Crystallogr. 2007; 40:658–674. [PubMed: 19461840]
33. Emsley P, Lohkamp B, Scott WG, Cowtan K. Features and Development of Coot. Acta Crystallogr. D Biol. Crystallogr. 2010; 66:486–501. [PubMed: 20383002]
34. Adams PD, Afonine PV, Bunkóczi G, Chen VB, Echols N, Headd JJ, Hung L-W, Jain S, Kapral GJ, Grosse-Kunstleve RW, McCoy AJ, Moriarty NW, Oeffner RD, Read RJ, Richardson DC, Richardson JS, Terwilliger TC, Zwart PH. The Phenix Software for Automated Determination of Macromolecular Structures. Methods. 2011; 55:94–106. [PubMed: 21821126]
35. Afonine PV, Grosse-Kunstleve RW, Echols N, Headd JJ, Moriarty NW, Mustyakimov M, Terwilliger TC, Urzhumtsev A, Zwart PH, Adams PD. Towards Automated Crystallographic Structure Refinement with Phenix.Refine. Acta Crystallogr. D Biol. Crystallogr. 2012; 68:352–367. [PubMed: 22505256]
36. Moriarty NW, Grosse-Kunstleve RW, Adams PD. Electronic Ligand Builder and Optimization Workbench (eLBOW): a Tool for Ligand Coordinate and Restraint Generation. Acta Crystallogr. D Biol. Crystallogr. 2009; 65:1074–1080. [PubMed: 19770504]
37. Knight Z, Feldman M, Balla A, Balla T, Shokat K. A Membrane Capture Assay for Lipid Kinase Activity. Nat Protoc. 2007; 2:2459–2466. [PubMed: 17947987]
38. Seiler CY, Park JG, Sharma A, Hunter P, Surapaneni P, Sedillo C, Field J, Algar R, Price A, Steel J, Throop A, Fiacco M, Labaer J. DNASU Plasmid and PSI:Biology-Materials Repositories: Resources to Accelerate Biological Research. Nucleic Acids Res. 2014; 42:D1253–D1260. [PubMed: 24225319]
39. Park J, Hu Y, Murthy TVS, Vannberg F, Shen B, Rolfs A, Hutti JE, Cantley LC, Labaer J, Harlow E, Brizuela L. Building a Human Kinase Gene Repository: Bioinformatics, Molecular Cloning, and Functional Validation. Proc. Natl. Acad. Sci. U.S.A. 2005; 102:8114–8119. [PubMed: 15928075]
40. Marukian S, Jones CT, Andrus L, Evans MJ, Ritola KD, Charles ED, Rice CM, Dustin LB. Cell Culture-Produced Hepatitis C Virus Does Not Infect Peripheral Blood Mononuclear Cells. Hepatology. 2008; 48:1843–1850. [PubMed: 19003912]
41. Cho N-J, Lee C, Pang PS, Pham EA, Fram B, Nguyen K, Xiong A, Sklan EH, Elazar M, Koytak ES, Kersten C, Kanazawa KK, Frank CW, Glenn JS. Phosphatidylinositol 4,5-Bisphosphate Is an HCV NS5A Ligand and Mediates Replication of the Viral Genome. Gastroenterology. 2015; 148:616–625. [PubMed: 25479136]
42. Laskowski RA, Swindells MB. LigPlot+: Multiple Ligand-Protein Interaction Diagrams for Drug Discovery. J Chem Inf Model. 2011; 51:2778–2786. [PubMed: 21919503]

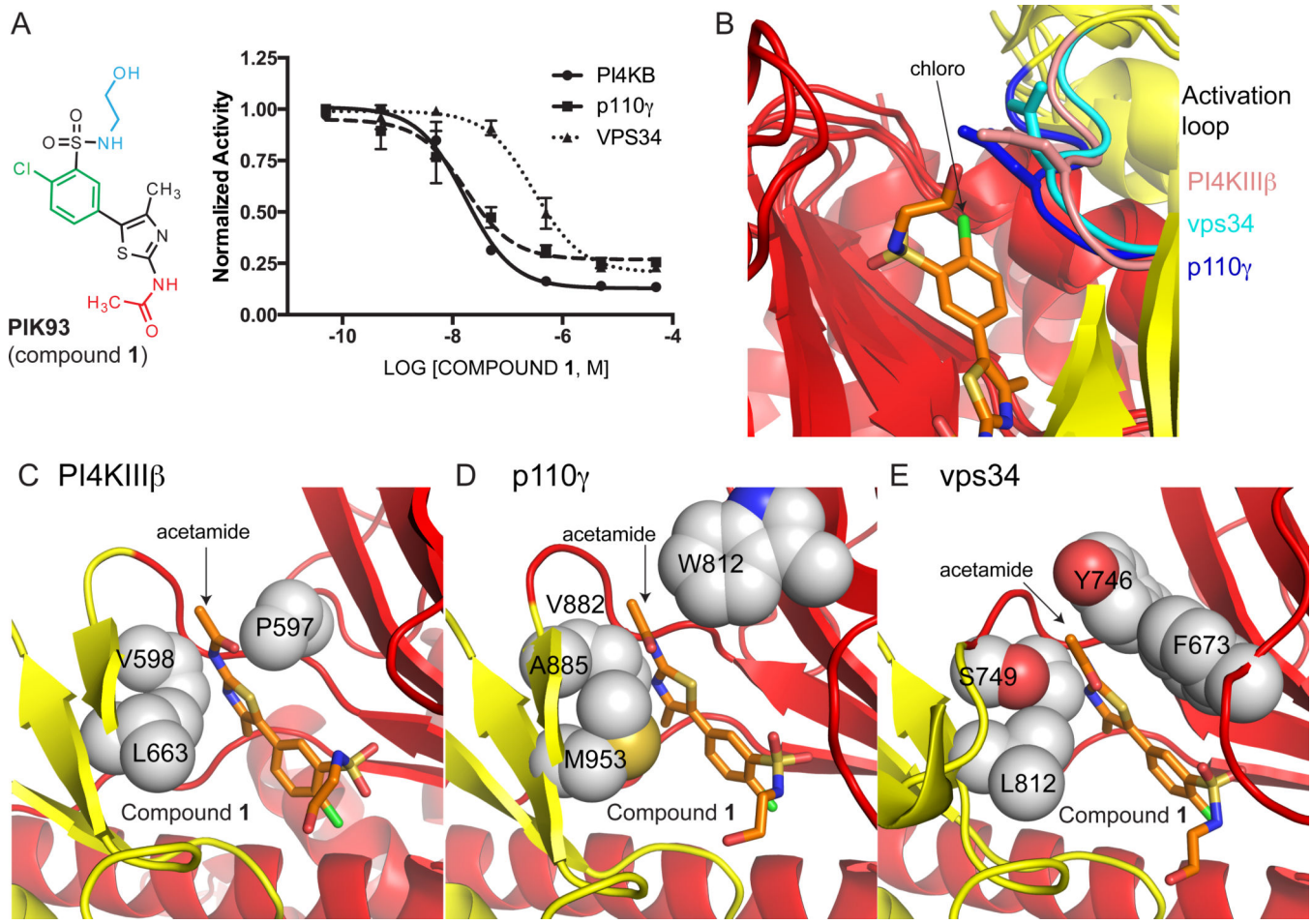

Figure 1. Structural basis for inhibition of PI4KIIIβ and PI3Ks by the inhibitor PIK93 (1)

A. Structure of compound **1**, with the ethanolamine substituent off the sulfonamide colored blue, the chloro substituent off the central phenyl colored green, and the acetamide substituent off the thiazol colored red. The potency of **1** against PI4KIIIβ, PI3Kγ, and vps34 is graphed.

B. The structures of PI4KIIIβ[18] (PDB ID:4D0L), vps34[19] (PDB ID: 2×6J), and PI3Kγ[16] (PDB ID: 2CHZ) bound to **1** aligned, showing the chloro substituent of **1** with the activation loop of each enzyme colored according to the legend.

C–E. The structures of PI4KIIIβ (C), PI3Kγ (D), and vps34 (E) with residues within 5 angstroms of the acetamide group of **1** shown as spheres.

A

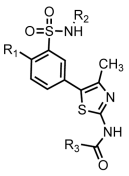

compound	R_1	R_2	R_3	compound IC_{50} (nM) PI4KIIIβ	PI3Kγ	PI3Kδ	VPS34	HCV Replication (nM) antiviral activity IC_{50}	cell viability CC_{50}
1	-Cl		-CH_3	17	17	77	307	4800	10,000
2	-Br		-CH_3	5.3	21	33	146	3000	5500
3	-OMe		-CH_3	4.4	181	223	>50,000	29,000	42,000
4	-Cl			5.5	3700	1570	>50,000	6800	33,000
5	-Cl			16	1500	340	>50,000	4400	20,000
6	-Cl	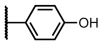	-CH_3	4.2	5.0	4.9	32	570	7000
7	-Cl	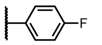	-CH_3	23	31	29	245.4	5900	13,000
8	-OMe			36	>50,000	50,000	>50,000	17,000	>40,000
9	-OMe	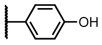		7	1046	152	>20,000	630	14,000
10	-OMe	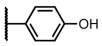		3.6	~20,000	720	>20,000	1300	32,000

B

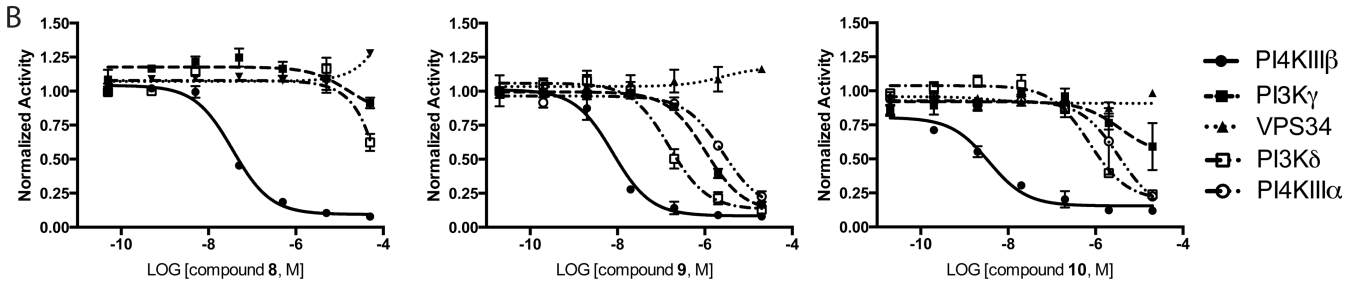

Figure 2. Development of novel PI4KIIIβ inhibitors

A. The structure of compound **1** is shown, with novel substituents at the R1, R2, and R3 position shown in tabular form, with the IC50 values for each compound against PI4KIIIβ, PI3Kγ, PI3Kδ and vps34 listed. Kinase assays were carried out in the presence of 10 μM ATP and 10mM $MgCl_2$ (PI4KIIIβ, PI3Kδ and PI3Kγ) or 10mM $MnCl_2$ (vps34). IC50 values measured using $MnCl_2$ are 10–20 fold higher than with the physiologically relevant $MgCl_2$ due to increased kinase activity. Inhibitors anti-HCV antiviral activity (IC50) was assessed by Gaussia luciferase assay (Gluc HCV2a activity) and cell viability (CC50) by Presto Blue assay (Gluc HCV2a viability), as described in the Experimental Section.

B. Full inhibitor curves for compound **8, 9**, and **10** are shown for PI4KIIIβ, PI3Kγ, PI3Kδ and vps34, with all measurements carried out in triplicate. For compounds **9** and **10** the curves for the related lipid kinase PI4KIIIα is shown as well, with assays against other related lipid kinases shown in Fig. S1.

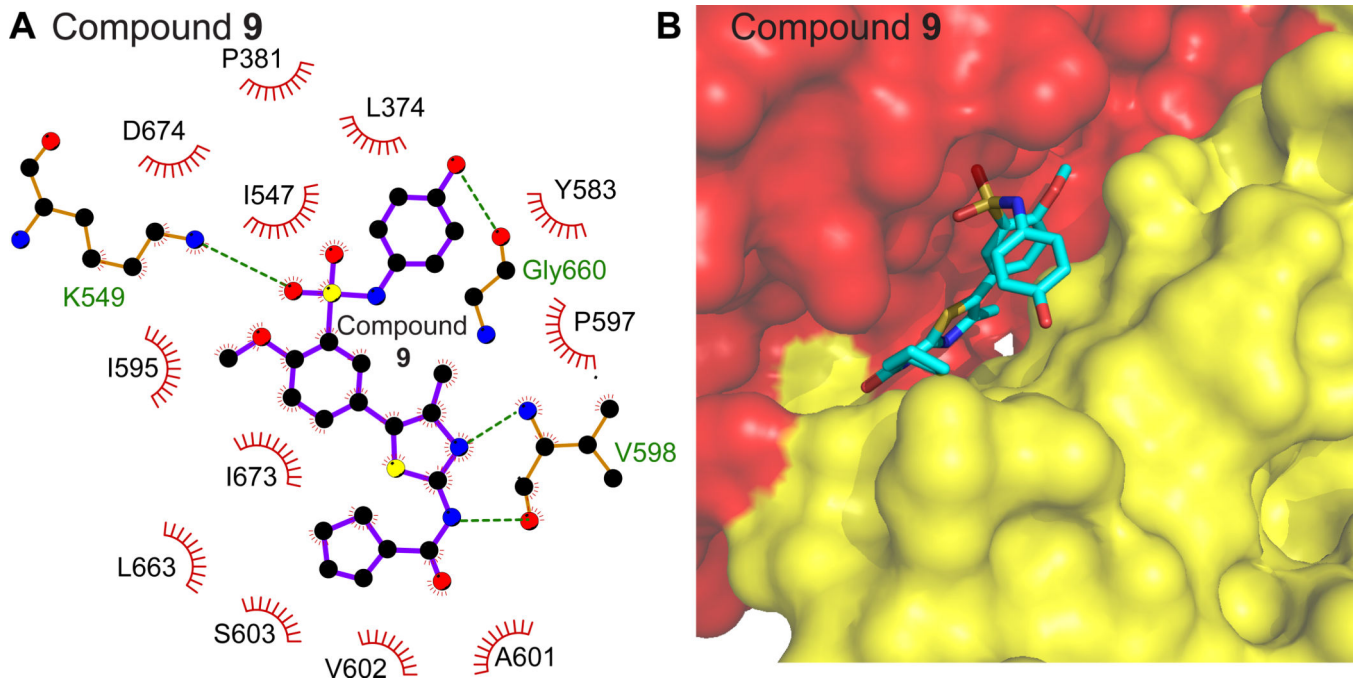

Figure 3. Structural basis of inhibition of PI4KIIIβ by compound 9

A. Residues mediating the interaction of PI4KIIIβ with compound **9** are shown, with putative hydrogen bonds indicated by dotted lines. Figure generated using ligplot [42].

B. The fit of compound **9** in the PI4KIIIβ active site pocket. The kinase domain is colored with the N-lobe shown in red, and the C-lobe shown in yellow.

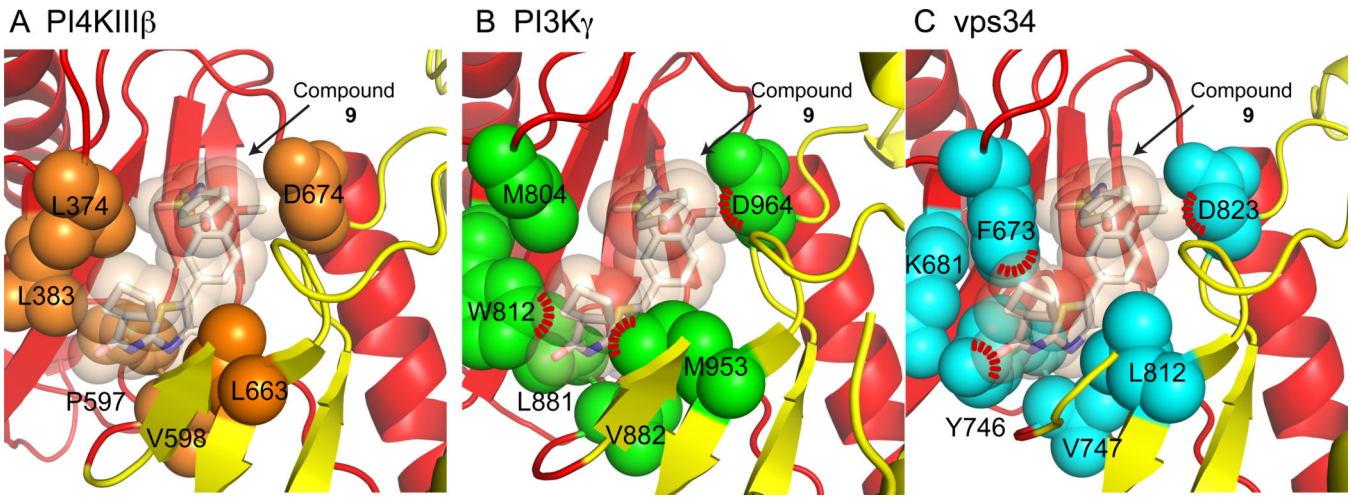

Figure 4. Structural basis for selectivity of compound 9

A. The structure of compound **9** bound to PI4KIIIβ, with selected residues colored in orange and shown as spheres.

B. A model of compound **9** in the active site of PI3Kγ. The model was generated by aligning the active site of the structure of compound **9** bound to PI4KIIIβ to the structure of PI3Kγ bound to compound **1** (PDB: 2CHZ). The equivalent residues shown in panel A are colored in green and shown as spheres, with steric clashes highlighted in red.

C. A model of compound **9** in the active site of vps34. The model was generated by aligning the active site of the structure of compound **9** bound to PI4KIIIβ to the structure of vps34 bound to compound **1** (PDB: 2×6J). The equivalent residues shown in panel A are colored in cyan and shown as spheres, with steric clashes highlighted in red.

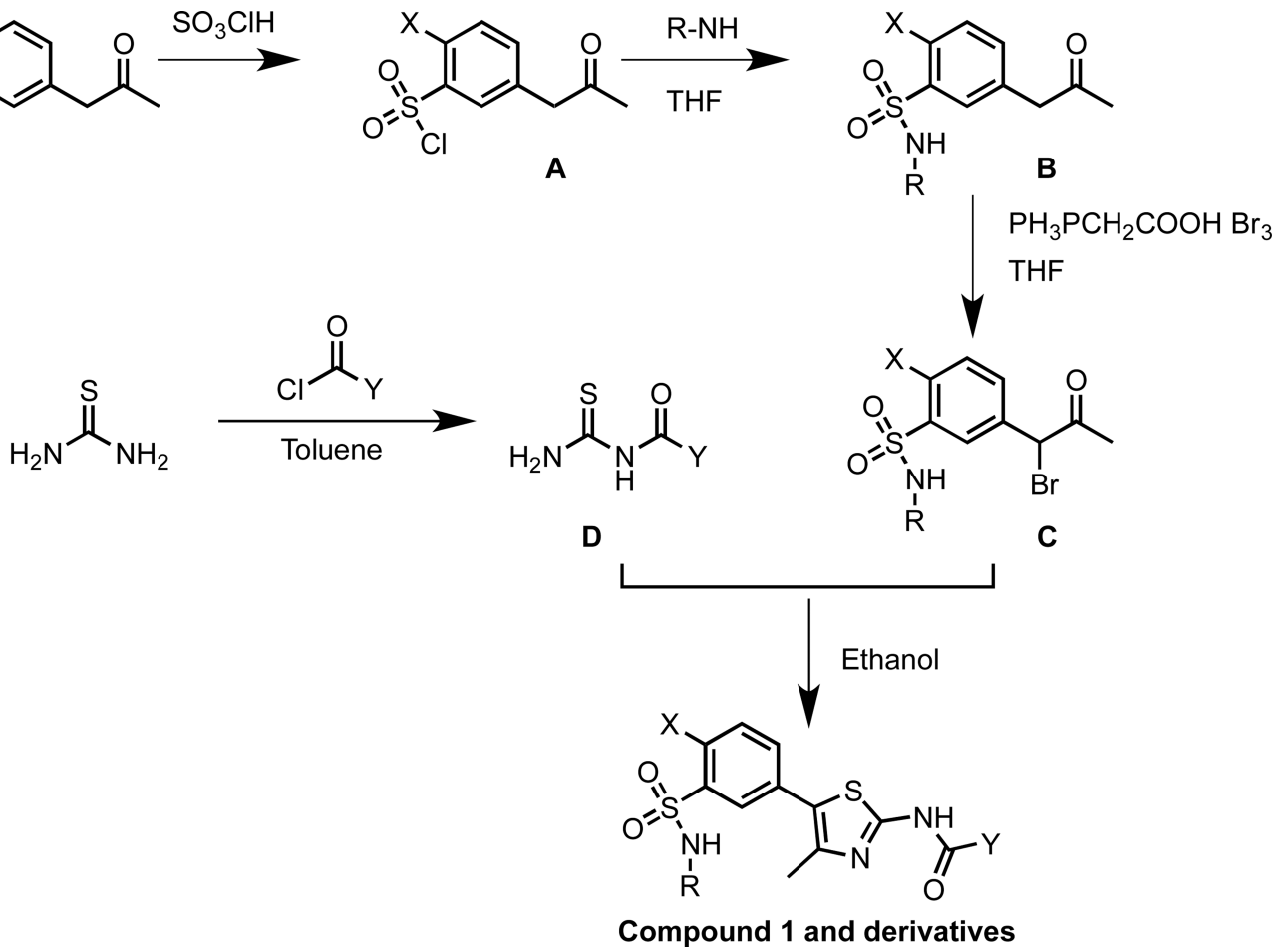

Scheme 1.
Synthesis of compound **1** and derivatives.

Table 1

Data collection and refinement statistics.

Data collection	**PI4K–Rab11-GDP-compound 9**
Wavelength (Ã)	0.9797
Space group	P 21 21 21
Unit cell	48.9 103.5 188.9, 90 90 90
Total reflections	67660 (6441)
Unique reflections	16316 (1611)
Multiplicity	4.1 (4.0)
Completeness (%)	98.63 (99.44)
Mean I/sigma(I)	8.93 (2.11)
Wilson B-factor	82.35
R-merge	0.1092 (0.7019)
R-meas	0.1249
CC1/2	0.993 (0.375)
CC*	0.998 (0.738)
Refinement	
Resolution range (Ã)	47.34 – 3.2 (3.31 – 3.2)
Reflections used for R-free	5%
R-work	0.2291 (0.3328)
R-free	0.2616 (0.3660)
Number of non-hydrogen atoms	5058
macromolecules	4987
ligands	71
water	0
Protein residues	621
RMS(bonds)	0.003
RMS(angles)	0.69
Ramachandran favored (%)	96
Ramachandran outliers (%)	0.3
Clashscore	5.73
Average B-factor	96
macromolecules	96.1
ligands	93.9

Statistics for the highest-resolution shell are shown in parentheses.